

1 **Competing multiple oxidation pathways shape**
2 **atmospheric limonene-derived organonitrates simulated**
3 **with updated explicit chemical mechanisms**

4 Qinghao Guo¹, Haofei Zhang², Bo Long³, Lehui Cui¹, Yiyang Sun¹, Hao Liu¹, Yixin
5 Liu¹, Yunting Xiao¹, Pingqing Fu¹ and Jialei Zhu^{1,*}

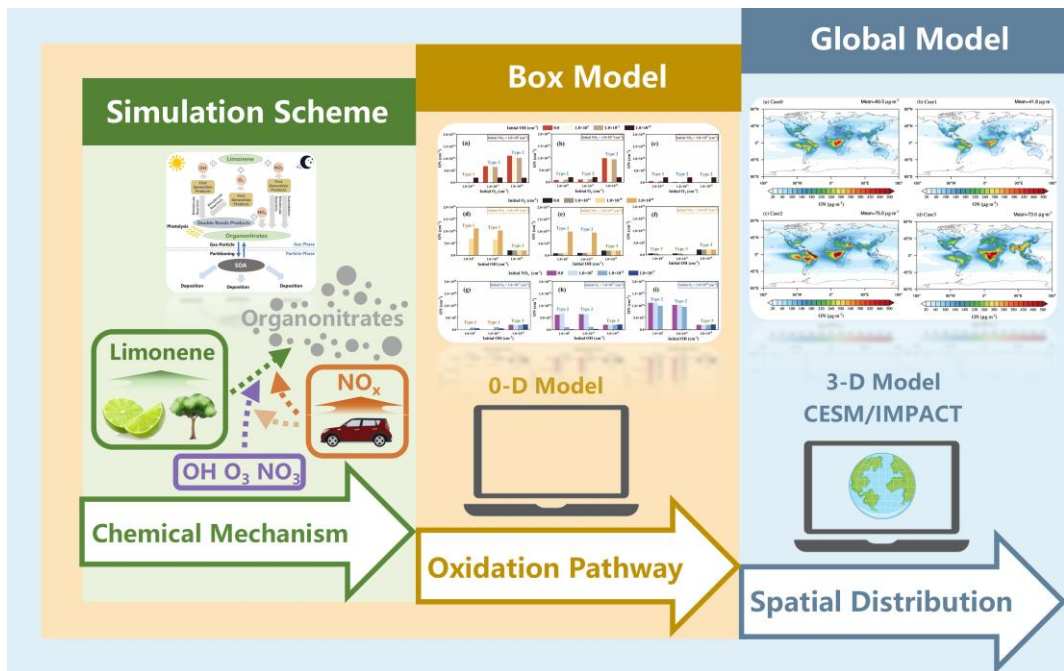
6 1 Institute of Surface-Earth System Science, School of Earth System Science, Tianjin University, Tianjin, 300072, China;

7 2 Department of Chemistry, University of California, Riverside, California 92521, USA;

8 3 College of Materials Science and Engineering, Guizhou Minzu University, Guiyang 550025, China.

9 *Correspondence to: Jialei Zhu, Email: zhujialei@tju.edu.cn*

10 **Abstract.** Organonitrates (ON) are key components of secondary organic aerosols (SOA) with potential
11 environmental and climate effects. However, ON formation from limonene, a major monoterpene with
12 unique structure, and its sensitivity to oxidation pathways remain insufficiently explored due to the
13 absence of models with explicit chemical mechanisms. This study advances the representation of
14 limonene-derived ON formation by incorporating 90 gas-phase reactions and 39 intermediates across
15 three oxidation pathways (O_3 , OH, NO_3) into both a chemical box model and a global model. Box model
16 sensitivity experiments revealed that competition among major oxidation pathways, coupled with the
17 high yield of limonene-derived ON from O_3 -initiated oxidation, leads to increased limonene-derived ON
18 production when the O_3 -initiated pathway is enhanced, whereas strengthening the OH- or NO_3 -initiated
19 pathways reduces ON formation. Compared to the box model, the global simulation exhibits stronger
20 nonlinear responses and great spatiotemporal variability in limonene-derived ON formation across
21 different oxidation pathways. This is primarily driven by the complex distribution of precursors and
22 oxidants, as well as changing in dominate chemical pathways under various meteorological conditions.
23 In the presence of the other two pathways, increasing the O_3 - or NO_3 -initiated oxidation pathway reduces
24 the global limonene-derived ON burden by 19.9% and 17.3%, respectively, whereas enhancing the OH-
25 initiated pathway increases it by 44.7%. limonene-derived ON chemistry developed in this study not only
26 enhances the global model's ability to simulate ON formation evaluated through comparison with
27 observations but also demonstrates an approach based on explicit chemical mechanisms that establishes
28 a methodological framework for simulating the chemical formation processes of SOA.



29

30 **1 Introduction**

31 Secondary organic aerosols (SOA) represent a substantial fraction of fine particulate matter and
 32 contribute to global public health risk, deterioration of air quality and climate change (Collaborators,
 33 2024; Lelieveld et al., 2015; Tao et al., 2017). Among chemical constituents, organonitrates (ON) are of
 34 particular interest owing to their large fraction in SOA (5%-77%) (Farmer et al., 2010; Kiendler-Scharr
 35 et al., 2016). The rate of particulate ON formation contributes strongly to the rate of SOA formation at
 36 night, which emphasizes the important roles of particulate ON in ambient SOA (Guo et al., 2024). The
 37 nitrate group in ON would influence the physical and chemical properties of SOA, such as decreasing
 38 saturated vapor pressure of the product molecule (Capouet and Müller, 2006). ON are secondary
 39 compounds formed via the oxidation of volatile organic compounds (VOCs) in the presence of nitrogen
 40 oxides (NO_x = NO + NO₂), substantially influencing NO_x cycling and formation of ozone (O₃) and
 41 HONO (Perring et al., 2013). In global scale, VOCs are mainly emitted from biogenic sources, while
 42 NO_x are emitted from a wide variety of anthropogenic sources (Ng et al., 2017; Glasius and Goldstein,
 43 2016). Therefore, a thorough investigation of ON is warranted to advance our understanding of
 44 interaction between biogenic and anthropogenic emissions.

45 The chemical formation mechanisms of ON are complex, hampering efforts to simulate and control
 46 SOA. In the daytime, hydroxyl radicals (OH) and ozone (O₃) oxidation of VOCs can produce peroxy

47 radical (RO_2), which reacts with NO_x to produce ON (Perring et al., 2013), while the reaction between
48 nitrate radicals (NO_3) and VOCs dominates the generation of ON in the nighttime (Rollins et al., 2009;
49 Perring et al., 2013; Ng et al., 2017). Furthermore, the coexistence among OH , O_3 and NO_3 has been
50 investigated in VOCs nocturnal oxidation (Brown and Stutz, 2012; Barber et al., 2018; Kwan et al., 2012;
51 Chen et al., 2022). Compared with single oxidant, the introduction of multiple oxidants leads to the
52 possible complex reaction mechanisms for VOCs. The regeneration of OH would change the O_3
53 oxidation process to form SOA (Sato et al., 2013). Chamber experiments show that SOA from NO_3
54 oxidation of VOCs are affected by oxidation of NO_2 by O_3 (Ng et al., 2017). Therefore, VOCs are
55 oxidized through the synergistic effects of multiple oxidants, driving the chemical formation of ON.
56 However, ON formation from the VOCs oxidation governed by mixing oxidants has not been fully
57 understood. In particular, the impact of oxidation pathways on the ON formation and spatial distribution
58 are still unclear.

59 As one of typical biogenic volatile organic compounds (BVOCs) (10% of monoterpenes), limonene
60 is mostly emitted from citrus plants and coniferous trees, with a total emission rate of $\sim 11 \text{ Tg}\cdot\text{yr}^{-1}$
61 (Guenther et al., 2012; Sindelarova et al., 2014). Limonene has a unique structure with an endocyclic
62 double bond and an exocyclic double bond, which makes it reactive towards atmospheric oxidants
63 (Surratt et al., 2008). Higher ON (30–72%) and SOA yields (17–40%) through NO_3 -initiated oxidation
64 of limonene than other monoterpenes have been observed in laboratory experiments (Fry et al., 2014;
65 Hallquist et al., 1999; Spittler et al., 2006; Moldanova and Ljungström, 2000; Fry et al., 2011). It has
66 been well demonstrated that limonene + NO_3 is most important pathway to form limonene-derived ON
67 (Kilgour et al., 2024; Ehn et al., 2014; Jokinen et al., 2015; Zhao et al., 2015). Furthermore, recent study
68 found the primary nitrooxy RO_2 formed through NO_3 addition to limonene occurs at both at endocyclic
69 double bond and the exocyclic double bond. These products could undergo autoxidation, which is fast
70 enough to RO_2 bimolecular reactions (Mayorga et al., 2022). The molecular compositions and formation
71 mechanism of limonene-derived ON have been well investigated through observations and laboratory
72 studies, while their description in models remains not explicit and advanced.

73 The early atmospheric model utilizes empirical yields and empirical coefficients for predicting
74 limonene-derived SOA production in simulation (Yu et al., 2019). Currently, chemical mechanisms are
75 simplified according to analogies with structurally similar compounds in most of regional and global

76 models due to simplicity and efficiency in calculation (Fisher et al., 2016; Li et al., 2023a). Nevertheless,
77 previous model studies have not included the formation mechanism of limonene-derived ON in detail
78 (Pye et al., 2015; Li et al., 2023a; Zare et al., 2019). Thus, incorporating explicit mechanisms is helpful
79 to understand limonene-derived ON formation process and the influence of interaction between multiple
80 oxidation pathways on ON formation.

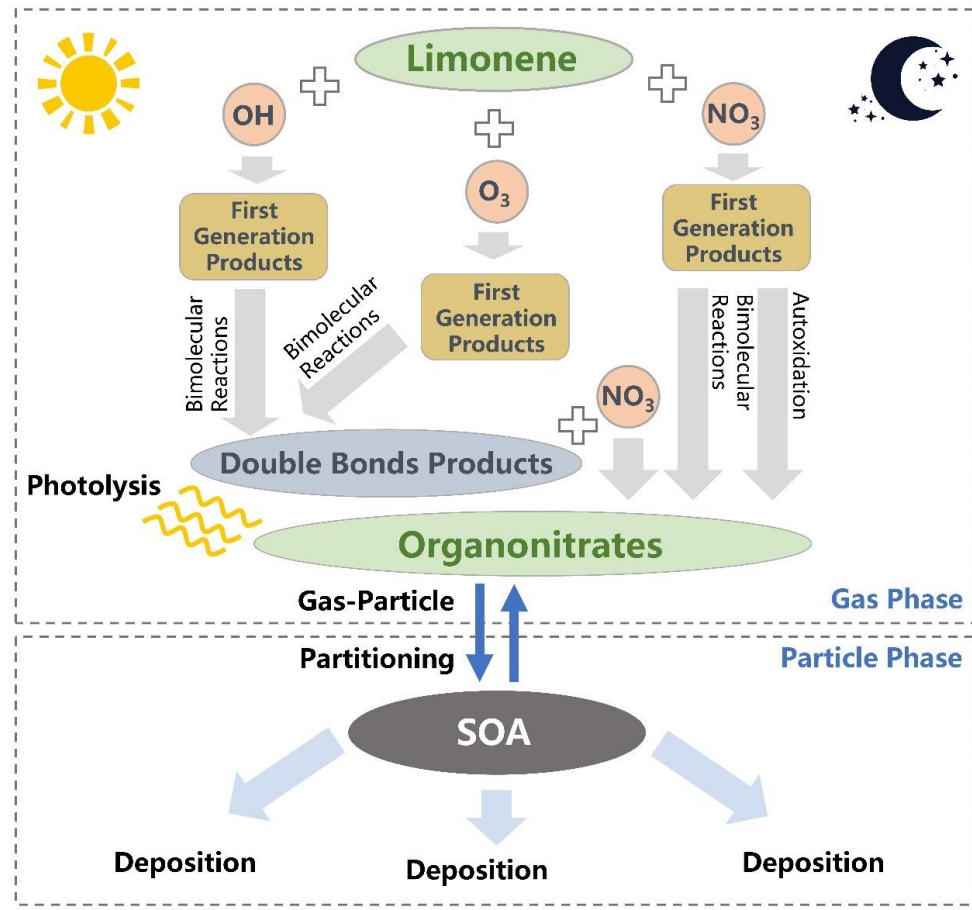
81 Herein, we investigated the impacts of multiple oxidation pathways on limonene-derived ON using
82 both chemical box model and global model, which were developed to include explicit chemical
83 mechanisms for limonene-derived ON formation. The effect of competition among individual oxidation
84 pathways on limonene-derived ON formation were discussed using a chemical box model based on
85 proposed mechanisms. The simulation framework of explicit chemical mechanisms was integrated into
86 global model to evaluate the spatial distributions of limonene-derived ON and contributions of individual
87 oxidation pathways. This study presents a numerical simulation framework for atmospheric chemical
88 processes and aims at enhancing the ability of models to simulate ON and understand the competition
89 effects among atmospheric oxidation pathways on SOA formation, improving atmospheric composition
90 forecasts and informing interaction between biogenic and anthropogenic emissions.

91 **2 Methodology**

92 **2.1 Limonene-derived ON formation mechanism**

93 In order to simulate ON via the gas-phase oxidation of limonene, the chemical mechanism used in our
94 model was updated with gas-phase chemical mechanisms of limonene-derived ON based on recent
95 laboratory studies (Mayorga et al., 2022) and Master Chemical Mechanism (MCM, v3.3.1). The explicit
96 chemical mechanism of limonene-derived ON involves three initial oxidation pathways: OH-, O₃- and
97 NO₃-initiated oxidation (Fig. 1). The detailed formulas of species could be found in Table S1. The
98 updated explicit formation mechanisms were list in Fig. S1 and Table S2. Compared to the MCM
99 mechanism, the chemical mechanism of limonene-derived ON formation used in this study is developed
100 to include: (1) NO₃ addition at three different carbonsites. Based on previous laboratory studies, the
101 exocyclic double bond oxidation branching ratio is ~0.03 (Fry et al., 2011; Donahue et al., 2007), while
102 the branching ratios of the two endocyclic C₁₀H₁₆NO₅-RO₂ isomers are 0.65:0.35 (Mayorga et al., 2022).
103 Thus, these branching ratios of the three C₁₀H₁₆NO₅-RO₂ isomers were used in our work. (2) Sequential

104 NO₃ oxidation reactions to form ON for all the products that contain double bonds from OH- and O₃-
105 initiated oxidation in MCM. The rate constants were set to be the same as those used in MCM for
106 limononaldehyde. (3) The formation of a ring-opened nitrooxy RO₂ in the presence of O₂ due to bond
107 scission of the two endocyclic nitrooxy RO, and its branching ratio was estimated (Draper et al., 2019;
108 Kurten et al., 2017; Guo et al., 2022). (4) H-shifts of the exocyclic C₁₀H₁₆NO₄-RO. (5) Bimolecular and
109 unimolecular reactions of the C₁₀H₁₆NO₆-RO₂ and C₁₀H₁₆NO₇-RO₂. The rate constants for the
110 bimolecular reactions are the same as those used in MCM, and autoxidation rate constants are calculated
111 by quantum chemical calculations (Mayorga et al., 2022). In addition, photolysis, widely recognized as
112 the predominant removal pathway of limonene-derived ON (Picquet-Varrault et al., 2020; Wang et al.,
113 2023), is included in our mechanism. While heterogeneous processes and hydrolysis of limonene-derived
114 ON are not included in our model, potentially resulting in a slight overestimation of simulated limonene-
115 derived ON concentrations, their contributions to ON removal are expected to be substantially smaller
116 than that of photolysis. Consequently, this omission introduces only minor uncertainties in our results.
117 In our explicit chemical mechanism, more intermediates and chemical processes of limonene-derived
118 ON were distinguished than simplified mechanisms used in previous models.



119

120 **Figure 1.** Schematic diagram of the limonene-derived ON formation pathways included in this work.

121 We assumed highly oxidized ON products ($C_{10}H_{13}NO_7$, $C_{10}H_{15}NO_4$, $C_{10}H_{15}NO_5$, $C_{10}H_{15}NO_6$,
 122 $C_{10}H_{15}NO_7$, $C_{10}H_{15}NO_8$, $C_{10}H_{17}NO_5$, $C_{10}H_{17}NO_6$, $C_{10}H_{17}NO_7$) to be semi- to low-volatile which can
 123 condense into the particulate phase upon formation. Their vapor pressures are estimated to calculate gas-
 124 particle partitioning (Table S3).

125 The vapor pressures of the above-mentioned ON species were estimated using two group contribution
 126 methods: EVAPORATION (Compernolle et al., 2011) and SIMPOL (Pankow and Asher, 2008). They
 127 are both widely used structure activity relationship (SAR)-based group contribution models to predict
 128 molecular vapor pressures. The key difference is that EVAPORATION considers proximity-based
 129 functional group interactions, so it considers differences in the locations of functional groups, while
 130 predictions from SIMPOL do not vary based on functional group locations. As a result, isomeric
 131 compounds with the same functional groups but different structures may have different predicted vapor
 132 pressures using EVAPORATION but the same using SIMPOL. Therefore, the EVAPORATION model

133 is preferred when chemicals structures are known while the SIMPOL model could be biased. In a recent
134 study, we showed that the EVAPORATION-based kinetic model predicts isoprene SOA more accurately
135 than the SIMPOL-based model, which underpredicts by ~ 20% (Shen et al., 2024).

136 In this work, because the chemical structures of the major ON species are known based on our recent
137 work (Mayorga et al., 2022), we adopted the EVAPORATION method in all our simulations. As the
138 EVAPORATION model input, the structures of the ON species from Mayorga et al. (2022) were
139 converted to SMILES strings. To illustrate the difference between the two models, the EVAPORATION-
140 predicted vapor pressures were compared with SIMPOL predictions (Table S3). The two methods predict
141 vapor pressures within one order of magnitude in most cases, which is typically considered acceptable
142 uncertainties for group contribution vapor pressure estimations.

143 **2.2 Chemical box model**

144 A zero-dimensional (0-D) chemical box model was used to examine the chemical processes of limonene-
145 derived ON, investigating the contributions of atmospheric oxidants and oxidant pathways. The chemical
146 mechanism presented in Fig. S1 and Table S2 was applied in this box model. To calculate the total
147 production of limonene-derived ON, processes such as photolysis, dilution, and deposition were ignored
148 for all chemical species in the model. The temperature was set to 298 K in the model. The initial
149 concentrations of limonene and other atmospheric components for all cases were set as shown in Table
150 S5. Limonene at a concentration of 1.0×10^{11} molecules·cm⁻³ was used as the precursor for ON, which
151 falls within the range of values reported in laboratory and observation studies (Guo et al., 2022; Luo et
152 al., 2023; Ham et al., 2016). The initial concentration of OH, O₃ and NO₃ spanned 1.0×10^5 to 1.0×10^{19}
153 molecules·cm⁻³, 1.0×10^{11} to 1.0×10^{18} molecules·cm⁻³ and 1.0×10^9 to 1.0×10^{17} molecules·cm⁻³,
154 respectively. The low values represent typical atmospheric concentrations of these species, which are
155 within the range of those reported in previous studies (Shen et al., 2021; Liu et al., 2023; Matsunaga and
156 Ziemann, 2019). The medium to high values represent extreme conditions, in order to investigate the
157 significant impact of oxidants on limonene-derived ON across a broad spectrum of oxidant levels.
158 Chamber experiments were simulated by the box model under ideal situation, which has been specifically
159 design to analyze chemical processes, while simulations under real atmospheric condition were carried
160 using global model in sect. 2.3. We conducted sensitivity tests (Sect. S1 in the supplement) to examine

161 oxidation pathways for formation of limonene-derived ON. Sensitivity tests under single initial oxidation
162 were set. Building upon this foundation, sensitivity tests with multiple oxidation pathways were
163 implemented: (1) introducing secondary oxidant across three concentration gradients under fixed primary
164 oxidant levels, followed by (2) increasing concentration of third oxidant with three concentration
165 gradients. A summary of all cases can be found in Table S4.

166 **2.3 Simulation of global limonene-derived ON**

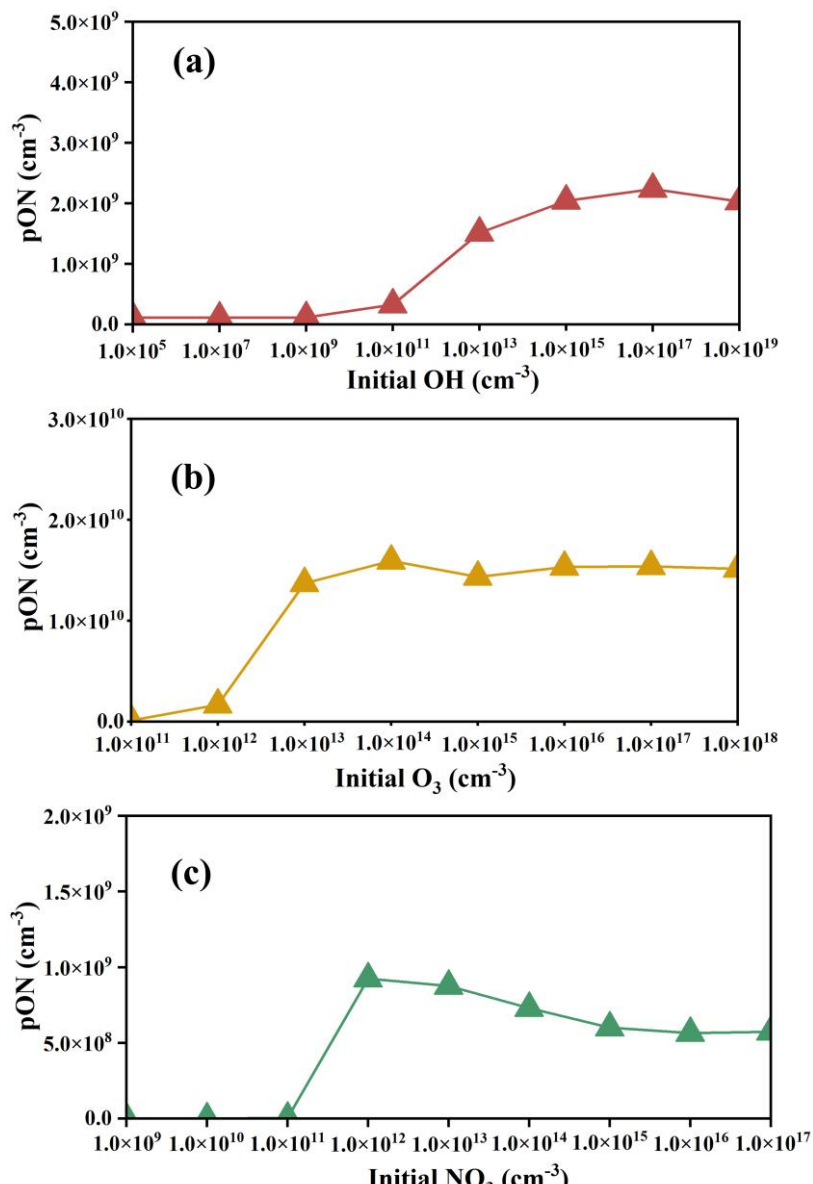
167 We used the Community Earth System Model (CESM) version 1.2.2.1 coupled with the University of
168 Michigan Integrated Massively Parallel Atmospheric Chemical Transport (IMPACT) aerosol model with
169 a resolution of $1.9^\circ \times 2.5^\circ$ for this study. The CESM/IMPACT model have included a fully explicit gas-
170 phase photochemical mechanism to predict the formation of semi-volatile organic compounds (SVOCs)
171 which then partition to an aerosol phase (Lin et al., 2014), facilitating the incorporation of explicit
172 limonene-derived ON mechanism to simulate their global burden. The IMPACT aerosol module gets the
173 meteorology field from the CESM model at each time step, while changes in the aerosols in IMPACT
174 do not provide feedback to the CESM. The emission of precursors BVOCs are estimated by the Model
175 of Emissions of Gases and Aerosols from Nature inventory (MEGAN) coupled to CESM/IMPACT
176 model. The developed explicit gas phase chemical mechanism same as used in above chemical box model
177 was applied to simulate the formation of limonene-derived ON. The highly oxidized limonene-derived
178 ON considered as semi-volatile species partitioning from gas phase to particle phase contributes to SOA.
179 A base case (Case0) was designed to simulate limonene-derived ON under all three initial oxidation
180 pathways, and six sensitivity experiments were designed for simulating global burden limonene-derived
181 ON under two initial oxidation pathways (Case 1-3) and single initial oxidation pathway (Case 4-6),
182 respectively. Above seven cases were summarized in Supplementary Sect. S2 and Table S6.

183 **3 Results and discussion**

184 **3.1 Limonene-derived ON formation through individual initial oxidation pathway.**

185 We employed a chemical box model to simulate limonene-derived ON formed through three initial
186 oxidation pathways, considering various oxidant concentrations (Fig. 2). These simulations were
187 designed to evaluate the effect of increasing oxidant concentrations on the yield of limonene-derived ON

188 from each initial oxidation pathway. In the case with individual OH oxidation pathway, the concentration
 189 of limonene-derived ON increases as the initial OH concentration increases (Fig. 2a), following a pattern
 190 to that of limonene consumption (Fig. S2a). Initial OH concentration increases from 1.0×10^5 to 1.0×10^{19}
 191 molecules \cdot cm $^{-3}$, resulting in \sim 20.0-fold increase in the production of limonene-derived ON. At this stage,
 192 limonene is not completely consumed by OH, indicating that higher initial OH concentration will
 193 increase consumption of limonene to produce more ON.



194
 195 **Figure 2.** Variations of limonene-derived ON in individual oxidation pathway under different oxidant concentrations.
 196 The triangles represent concentration of limonene-derived ON in each experiment. The lines represent the trend of
 197 limonene-derived ON. The three datapoint colors represent three initial oxidation pathways (red for OH-initiated
 198 oxidation, yellow for O₃-initiated oxidation, green for NO₃-initiated oxidation).

199 In the case with individual O_3 oxidation pathway, the limonene-derived ON increases first and then
200 maintains a relatively stable production with the increase of initial O_3 concentration (Fig. 2b). Limonene
201 is not completely consumed when initial O_3 concentrations below 1.0×10^{14} molecules \cdot cm $^{-3}$. Increased
202 consumption of limonene lead to an increase in ON production with increased O_3 concentration.

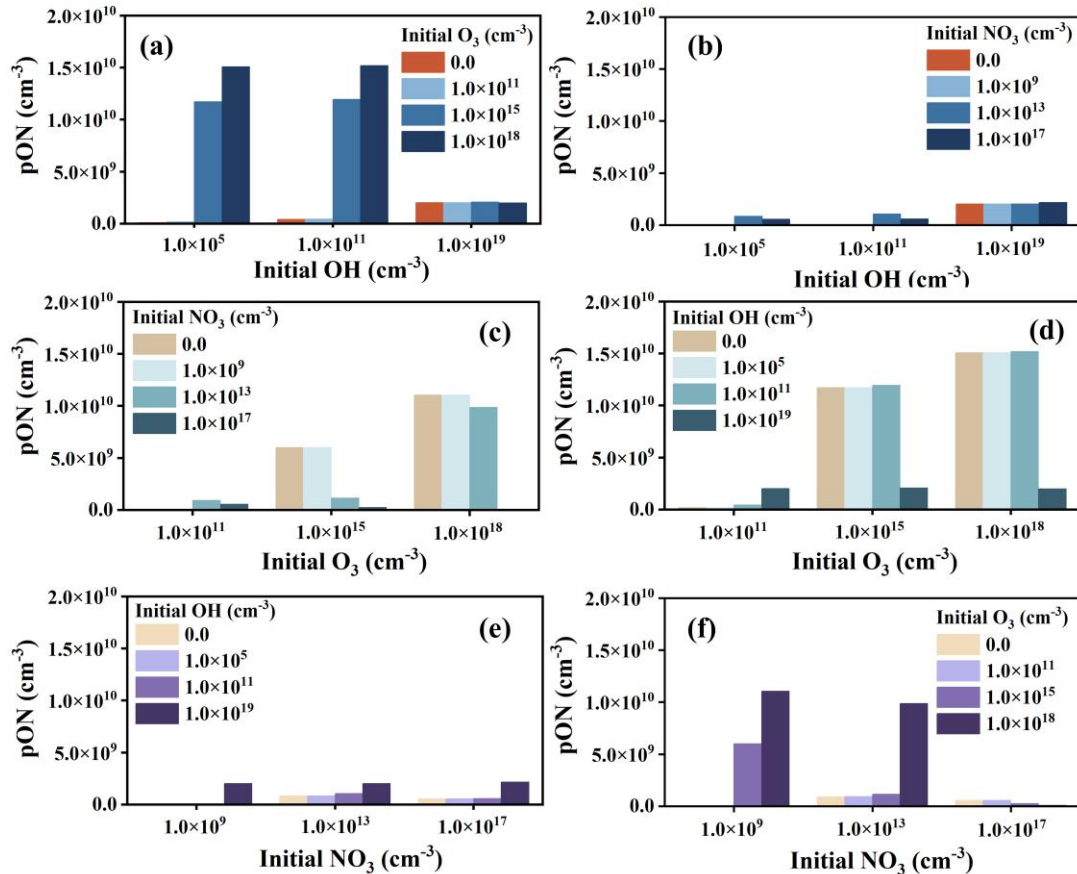
203 Same to the cases of the OH- and O_3 -initiated oxidation pathways, limonene-derived ON increases
204 when initial NO_3 concentrations below 1.0×10^{12} molecules \cdot cm $^{-3}$ could be caused by incompletely
205 consumed limonene (Fig. 2c). The increased consumption of limonene with increase in concentrations
206 of NO_3 lead to the increased production of ON. However, different from the cases of OH- and O_3 -initiated
207 oxidation pathways, as initial NO_3 concentrations continued to increase, limonene-derived ON
208 production decrease. When limonene-derived ON concentrations reached steady state within 30 minutes,
209 compared to the case with initial NO_3 concentration of 1.0×10^{12} molecules \cdot cm $^{-3}$, reaction of LIMAL and
210 NO_3 become the dominant pathway in the case with initial NO_3 concentration of 1.0×10^{17} molecules \cdot cm $^{-3}$. The lower yield of the NO_3 oxidation pathway (9.2%) of LIMAL relative to OH oxidation pathway
211 (28.8%) results in decreased limonene-derived ON (green box in Fig. S1). The results mean that at low
212 initial oxidant concentration, limonene-derived ON shows a strong dependence on initial oxidant
213 concentration, and the dependence on intermediate reaction rates becomes more important at high initial
214 oxidant concentration.

216 In addition, average concentration of ON of OH-, O_3 - and NO_3 -initiated oxidation pathways when
217 oxidations are sufficient are calculated separately. The O_3 -initiated oxidation pathway (1.5×10^{10}
218 molecules \cdot cm $^{-3}$ limonene-derived ON produced) yields more ON than the OH- (2.1×10^9 molecules \cdot cm $^{-3}$
219 limonene-derived ON produced) and NO_3 -initiated (7.1×10^8 molecules \cdot cm $^{-3}$ limonene-derived ON
220 produced) oxidation pathways when limonene initial concentration is constant. This indicates that under
221 initial conditions with sufficient oxidation, O_3 -initiated oxidation pathway of limonene has highest yield
222 of ON, which is about 15.0%, while that is low by OH- (2.1%) and NO_3 -initiated (0.7%) oxidation
223 pathway. This difference in the ON yield among various oxidation pathways will be used to explain the
224 contributions of each oxidation pathway to ON concentration in the following discussion.

225 **3.2 Effects of multiple oxidation pathways on limonene-derived ON formation.**

226 Compared to the simulation scheme with individual oxidation pathway discussed above, introducing
227 multiple oxidation pathways leads to comprehensive competition among them, which results in a
228 nonlinear response of ON concentration to changes in the initial concentrations of oxidants. Figure 3
229 shows the dependence of limonene-derived ON on initial concentration of oxidants when include two
230 initial oxidation pathways. The addition of oxidants has various effects on the yield of limonene-derived
231 ON. When the initial concentration of oxidant is low (1.0×10^5 molecules·cm⁻³ for OH, 1.0×10^{11}
232 molecules·cm⁻³ for O₃, 1.0×10^9 molecules·cm⁻³ for NO₃), the initial limonene will not be completely
233 consumed. In all case with low concentration of oxidants, adding another oxidant with oxidation pathway
234 will increase consumption of limonene, leading to increase in the limonene-derived ON production.
235 When the initial concentration of oxidants is high, limonene will be nearly or completely consumed. In
236 these cases, the production of limonene-derived ON will be determined by the competition between the
237 two oxidation pathways. The product of limonene-derived ON steadily increased as the initial
238 concentration of O₃ increases from 0 to 1.0×10^{18} molecules·cm⁻³ when the initial concentration of OH or
239 NO₃ is constant (Fig. 3a, f). According to the chemical mechanism applied in the model, the reaction
240 between limonene and O₃ has higher rate than OH and NO₃ in these cases (Table S7). As a result, in the
241 presence of O₃, the oxidation of limonene with O₃ proceeds more rapidly than with OH or NO₃, leading
242 to higher concentration of limonene-derived ON due to the high yield of O₃ oxidation pathway as
243 discussed in above section (compare Fig. 2b with Fig. 2a and 2c). In contrast, compared to only including
244 O₃ oxidation pathway, adding oxidation pathways with OH or NO₃ will result in a decrease in limonene-
245 derived ON production (Fig. 3c, d), because some limonene that would have reacted with O₃ is instead
246 converted to ON through the OH or NO₃ pathways with lower yield. Therefore, the dominant oxidation
247 pathway and its ON yield determine the impact of the competition between the two oxidation pathways
248 on the final limonene-derived ON production. A similar phenomenon observed in laboratory study shows
249 that NO_x influences γ -terpinene ozonolysis by enhancing NO₃ production at high NO_x levels, which
250 subsequently leads to NO₃ preferentially consuming γ -terpinene over O₃ (Xu et al., 2020), illustrating
251 the competition between oxidants. The addition of the OH-initiated oxidation pathway results in a small
252 increase in ON production compared to NO₃-initiated oxidation alone (Fig. 3e), due to the slightly higher
253 yields of limonene-derived ON for OH-initiated oxidation pathway. The ON production would not

254 change much when add the NO_3 -initiated oxidation pathway compared to the case with OH -initiated
 255 oxidation pathway alone (Fig. 3b) because of unchanged the main initial oxidation pathway. These
 256 sensitivity experiments suggest that competition of oxidation pathways plays an important role in
 257 formation of limonene-derived ON.

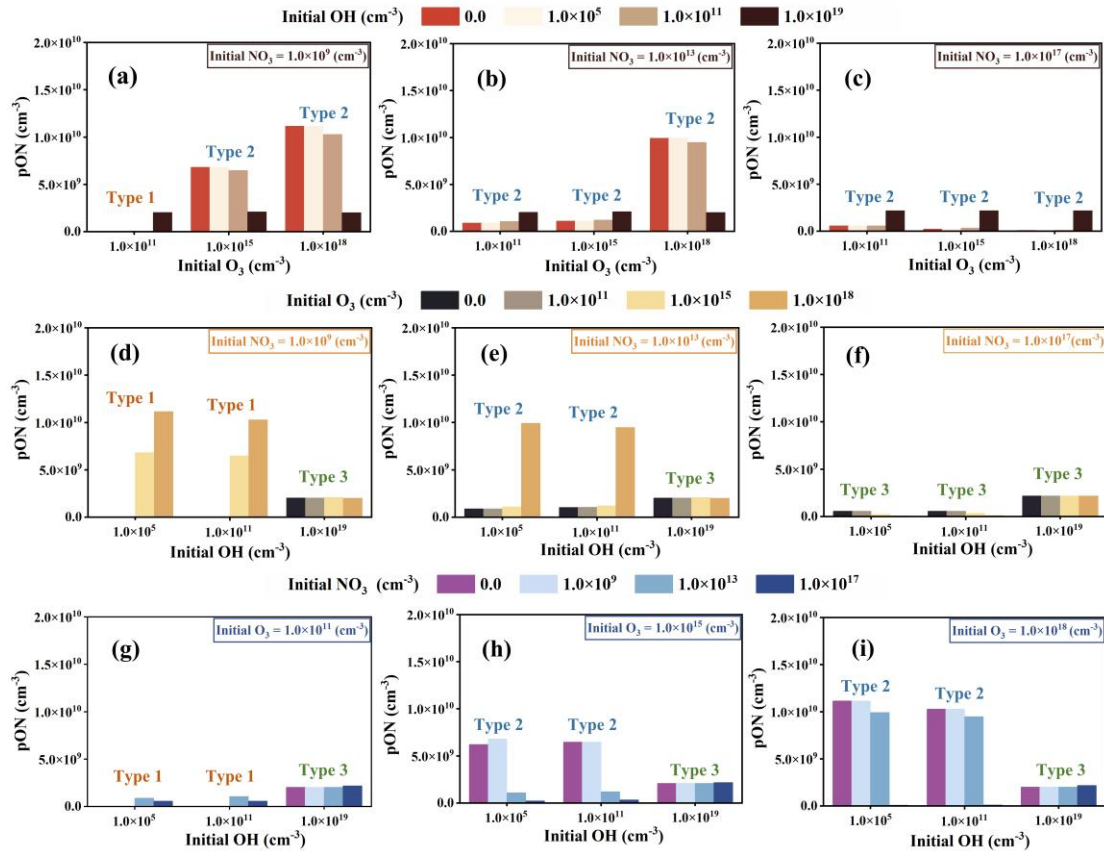


258

259 **Figure 3.** Simulated limonene-derived ON in two initial oxidation pathways under different oxidant conditions,
 260 including variation of production of limonene-derived ON with adding (a) initial O_3 concentration and (b) initial
 261 NO_3 concentration in the three OH levels; variation of limonene-derived ON production with adding (c) initial OH
 262 concentration and (d) initial NO_3 concentration in the three O_3 levels; variation of limonene-derived ON production
 263 with adding (e) initial OH concentration and (f) initial O_3 concentration in the three NO_3 levels.

264 Based on the production variations of limonene-derived ON in the cases with one and two initial
 265 oxidation pathways discussed above, the comprehensive impact of multiple oxidants on limonene-
 266 derived ON formation in the cases with multiple initial oxidation pathways are analyzed (Fig. 4). The
 267 results can be summarized into three types. The Type 1 is the cases when limonene is not completely
 268 consumed (Fig. S4). When two initial oxidant concentration is low (Fig. 4a, d, g) and medium (Fig. 4d,
 269 g), the addition of third oxidant increases the production of limonene-derived ON because the addition

270 of the third oxidant increases consumption of limonene. If the oxidant concentration is sufficient to
271 consume up limonene, the production of limonene-derived ON will be determined by the competition
272 between initial oxidation pathways. The Type 2 is the cases with large changes of limonene-derived ON.
273 Under low NO_3 and moderate and high O_3 conditions, the production of limonene-derived ON decreases
274 with adding OH (Fig. 4a, b), because some limonene that would have reacted with O_3 is instead converted
275 to ON through the OH pathways with lower yield. The formation of limonene-derived ON shows similar
276 pattern for Type 2 in Figure 4h and i. On the one hand, the yield of limonene-derived ON from NO_3 -
277 initiated oxidation is lowest, so the production of limonene-derived ON will decrease when the formation
278 of limonene-derived ON from this pathway becomes the dominant formation route. On the other hand,
279 adding NO_3 -initiated oxidation pathway also consumes NO_3 that would have reacted with the product of
280 the OH- and O_3 -initiated oxidation, resulting in decrease production of limonene-derived ON. The
281 changes in ON production with constant initial concentration of limonene and various oxidation
282 pathways indicate the interactions of different oxidation process of limonene. In contrast to OH- and
283 NO_3 -initiated oxidation pathway, adding oxidation pathways with O_3 will result in increase in limonene-
284 derived ON production (Fig. 4e), due to higher yield of limonene-derived ON from O_3 -initiated oxidation
285 pathway than OH- and NO_3 -initiated oxidation pathways. Since the yield of limonene-derived ON of OH-
286 initiated oxidation is higher than NO_3 -initiated oxidation, the production of limonene-derived ON
287 decreases (Fig. 4c) as the main oxidation pathway changes from NO_3 to OH oxidation (Table S8).
288 Additionally, in some sensitivity experiments (Fig. 4d-i), ON concentration do not change much with the
289 addition of an oxidation pathway (Type 3). This could be explained by minimal competition with the
290 rapid main oxidation pathway. These sensitivity experiments suggest that the limonene-derived ON
291 production in the simulated system are not only controlled by limonene concentration, but also affected
292 by synergic effect of multiple oxidants and oxidation pathways.



293

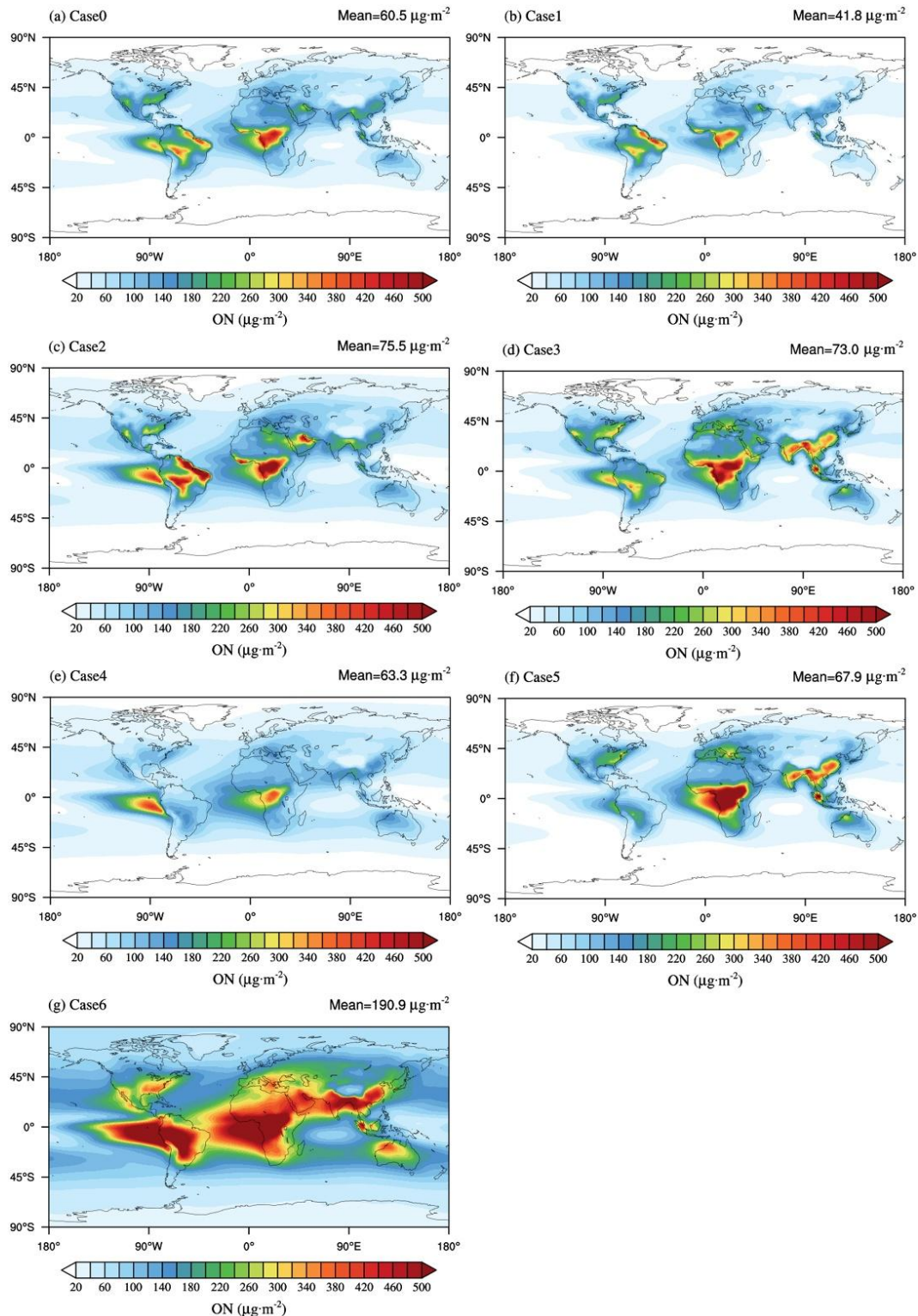
294 **Figure 4.** The influence of adding OH-, O_3 - and NO_3 -initiated oxidation pathways on the production of limonene-
295 derived ON under different oxidant conditions, including variation of limonene-derived ON production with adding
296 initial OH concentration in the three O_3 levels under (a) low, (b) moderate and (c) high NO_3 levels; variation of
297 limonene-derived ON production with adding initial O_3 concentration in the three OH levels under (d) low, (e)
298 moderate and (f) high NO_3 levels; variation of limonene-derived ON production with adding initial NO_3
299 concentration in the three OH levels under (d) low, (e) moderate and (f) high O_3 levels. In each panel, the types
300 marked on the columns show the cases when limonene is not completely consumed (type 1) and almost completely
301 consumed (large (type 2) and small (type 3) changes in limonene-derived ON production).

302

3.3 Contribution of each oxidation pathway to global limonene-derived ON.

303 Global simulation using CESM/IMPACT model was performed to characterize the spatial and temporal
304 distribution of limonene-derived ON and the contributions of each oxidation pathway to global burden.
305 Incorporation of formation of limonene-derived ON reduces underestimation of simulated ON by
306 comparison with observations summarized in the literature (Sect. S3 in the supplement) (Li et al., 2023b).
307 The spatial distribution of limonene-derived ON is shown in Fig. 5a. The simulated global mean
308 limonene-derived ON burden is about $60.5 \mu\text{g} \cdot \text{m}^{-2}$, and the highest burdens ($>500 \mu\text{g} \cdot \text{m}^{-2}$) are predicted
309 over tropical forest regions of central Africa. As the primary precursor of limonene-derived ON, the
310 concentration of limonene dominates the yield of these ON compounds. The seasonal cycle of simulated
311 limonene-derived ON is presented in Fig. S6, which is mainly depend on limonene levels. Global average

312 limonene-derived ON burden peaks in the summer ($69.2 \mu\text{g}\cdot\text{m}^{-2}$) due to highest global average limonene
313 concentration (Fig. S7b), while the large burden of limonene-derived ON in fall is driven by the presence
314 of both high limonene concentration (Fig. S7c) and NO concentration (Fig. S8c) compared to spring and
315 winter. In contrast, the burden of limonene-derived ON is lowest in winter ($48.1 \mu\text{g}\cdot\text{m}^{-2}$) because of
316 lowest concentration of limonene (Fig. S7d). Beyond the effects of limonene and NO concentrations,
317 oxidant levels and oxidation pathways also affect the formation mechanisms and production of limonene-
318 derived ON, which may explain the highest burden in regions such as Central Africa, rather than Amazon
319 where limonene concentrations are highest over the world (Fig. S9a). The concentration of oxidants is
320 inherently low in Amazon (Fig. S9b-d) and oxidant scavenging in the presence of isoprene with high
321 concentrations greatly reduce the photochemical formation of limonene-derived ON (McFiggans et al.,
322 2019). Thus, oxidant competition with isoprene leads to low burden of limonene-derived ON in Amazon
323 despite the highest burden of limonene there. Therefore, high concentrations of limonene-derived ON
324 can only form when both high limonene and oxidant concentrations are present simultaneously.



325

326 **Figure 5.** Annual mean column concentration of limonene-derived ON with different simulation schemes. (a) Run
327 with three initial oxidation pathways (Case0), (b) without OH-initiated oxidation pathway (Case1), (c) without O_3 -
328 initiated oxidation pathway (Case2), (d) without NO_3 -initiated oxidation pathway (Case3), (e) without O_3 - and NO_3 -
329 initiated oxidation pathways (Case4), (f) without OH- and NO_3 -initiated oxidation pathways (Case5) and (g) without
330 OH- and O_3 -initiated oxidation pathway (Case6).

331 To quantify the contribution of each oxidation pathway to the formation of limonene-derived ON in
332 different regions, we conducted a series of sensitivity experiments (Case1 to 6 introduced in method
333 section) on the oxidation pathways (Fig. 5b-g). Our simulations indicate that increasing O_3 and NO_3^- -
334 initiated oxidation pathways result in 15.5% and 18.0% increase of global average burden of limonene-
335 derived ON, respectively, compared to OH-initiated oxidation pathway alone (Fig. S10a, b). This is
336 primarily because higher yields of limonene-derived ON associated with the O_3 - and NO_3^- -initiated
337 oxidation pathways compared to OH-initiated oxidation pathways. When compared to O_3 -initiated
338 oxidation pathway alone (Fig. S10c, d), the addition of OH- or NO_3^- -initiated pathways result in increased
339 burden of limonene-derived ON in the limonene-sufficient region (e.g. Amazon), owing to adding a
340 limonene-derived ON formation pathway to consume more limonene. However, in the limonene-
341 deficient yet NO_3^- -sufficient regions (e.g. Central Africa, Mediterranean, and middle and low latitude of
342 Asia), increasing the OH- or NO_3^- -initiated oxidation pathways reduces the burden of limonene-derived
343 ON. This occurs because the oxidation of limonene by OH or NO_3^- suppresses O_3 -initiated oxidation,
344 which otherwise produces limonene-derived ON with a high yield. Additionally, if limonene undergoes
345 oxidation by NO_3^- , the availability of NO_3^- for the nitration of OH- and O_3 -initiated oxidation products of
346 limonene will decrease, resulting in a reduction in limonene-derived ON. The addition of OH- and O_3 -
347 initiated oxidation pathways reduces global average burden of limonene-derived ON by 60.5% and 78.1%
348 respectively, compared to the case with NO_3^- -initiated oxidation pathway alone (Fig. S10e, f). This
349 reduction is likely due to insufficient NO_3^- oxidation at night to further oxidize intermediates produced
350 from OH- and O_3 -initiated limonene oxidation during the day, limiting the formation of limonene-derived
351 ON at night.

352 The burden of limonene-derived ON undergoes a noticeable change when an additional oxidation
353 pathway is introduced to the existing two pathways (Fig. S11). Adding OH-initiated oxidation pathway
354 increases the global average burden of limonene-derived ON from 41.8 to $60.5 \mu\text{g}\cdot\text{m}^{-2}$, by 44.7%, while
355 adding O_3 -initiated oxidation pathway decrease that from 75.5 to $60.5 \mu\text{g}\cdot\text{m}^{-2}$, by 19.9% (Fig. S11a, b),
356 which was attributed to the competition between the OH and O_3 oxidation pathways for reactions with
357 limonene. Compared to the simplified condition in simulation using chemical box model, global
358 simulation considers diurnal variations of oxidation. When the O_3 -initiated oxidation pathway produces
359 the same amount of limonene-derived ON as the OH-initiated pathway, it consumes more NO_3^- . As a

360 result, increasing the O_3 oxidation pathway reduces the availability of NO_3 for the nitration of
361 intermediate oxidation products in the nighttime, thereby lowering the total limonene-derived ON yield
362 across all three pathways. In contrast, enhancing the OH oxidation pathway increases the total yield.
363 Moreover, the addition of the NO_3 -initiated oxidation pathway increases burden of limonene-derived ON
364 in the limonene-sufficient region even over $150 \mu\text{g}\cdot\text{m}^{-2}$ (Fig. S11c). However, in the region with high
365 NO_3 concentration, the burden of limonene-derived ON decreases (Fig. S11c) because the NO_3 -initiated
366 oxidation pathway yields less limonene-derived ON than the O_3 - and OH-initiated oxidation pathways.
367 These results highlight the different nonlinear responses of limonene-derived ON to multiple oxidation
368 pathways under varying oxidation conditions and precursor concentrations. This discrepancy highlights
369 differences between global-scale dynamics and idealized box model conditions, emphasizing the
370 importance of developing explicit chemical mechanisms in global models for understanding SOA
371 formation processes. Prior laboratory study has also demonstrated that investigating the response of ON
372 reveals complex and nonlinear behaviour with implications that could inform expectations of changes to
373 ON concentrations as efforts are made to reduce oxidant concentrations (Mayhew et al., 2023).

374 **4 Conclusion and implications**

375 In this work, the explicit chemical mechanism is developed to simulate formation and spatial distribution
376 of limonene-derived ON using a chemical box model and global model CESM/IMPACT. Under multiple
377 initial oxidation pathways, limonene-derived ON shows non-linear variations with different oxidant
378 conditions, which is controlled by the synergetic effects of multiple oxidants. When limonene is not
379 consumed, adding another oxidant with oxidation pathway will increase limonene-derived ON due to
380 increased consumption of limonene. When limonene is completely consumed, limonene-derived ON
381 production is dominated by competition of oxidation pathways. The production of limonene-derived ON
382 is increased by O_3 -initiated oxidation pathway while decreased by OH and NO_3 -initiated oxidation
383 pathway. This is mainly because limonene oxidated by O_3 produces more ON than OH and NO_3 , resulting
384 from the simulation under individual initial oxidation pathway.

385 The global model simulation indicates that oxidation process is important for limonene-derived ON
386 formation in addition to limonene concentration. Global limonene-derived ON burden decreases by 19.9%
387 and 17.3% due to O_3 - and NO_3 -initiated oxidation pathway, while OH-initiated oxidation pathway

388 increases global limonene-derived ON burden by 44.7% compared the case only including the other two
389 oxidation pathways. These differences can be attributed to the complex nonlinear response of limonene-
390 derived ON yield to different reaction pathways under varying precursor and oxidant conditions.

391 The chemical mechanism of ON formation may influence the formation and spatial distribution of
392 ON. We only include main oxidation process published to date in the model, while some pathways (i.e.
393 Heterogeneous NO_3 reactions) of ON is missing in this work. Gas-phase oxidation in our mechanism is
394 considered as the dominant formation pathway of ON (Fan et al., 2022; Perring et al., 2013). Future
395 inclusion of newly identified and quantified ON chemistry may lead to unpredictable nonlinear impacts
396 on simulation outcomes. Although uncertainties remain in simulating limonene-derived ON due to
397 limited knowledge of its formation mechanism, this work offers an improvement in the global model's
398 ability to simulate ON and presents a methodological framework for simulating SOA and their chemical
399 processes. This framework can be used in the future to improve SOA burden predictions and provide a
400 comprehensive understanding of the complex interactions between multiple oxidation pathways, which
401 are crucial for SOA formation (Chen et al., 2022; Zang et al., 2024). Quantitative understanding of these
402 complex interactions in contributing to SOA formation can definitely facilitate better understanding the
403 contributions of interactions and antagonistic actions between anthropogenic and natural emissions to
404 atmospheric aerosols. These works provide valuable insights for making more effective secondary
405 aerosol pollution control strategies to improve air quality.

406 **Data availability.** Simulation data are available upon request to the corresponding authors.

407 **Author contributions.** QG and JZ designed the study, developed the chemical box model and global
408 model conducted the simulations, analyzed the data, and wrote the manuscript. HZ and BL provided the
409 laboratory data. PF, LC, YS, HL, YL and YX contributed to the discussion and revision of the paper.

410 **Competing interests.** The authors declare no competing financial interest.

411 **Disclaimer.** Publisher's note: Copernicus Publications remains neutral with regard to jurisdictional
412 claims in published maps and institutional affiliations.

413 **Acknowledgments.** The authors acknowledge the financial support of the National Natural Science
414 Foundation of China.

415 **Financial support.** This study was supported by the National Natural Science Foundation of China
416 (Grant 42177082).

417 **References**

418 Barber, V. P., Pandit, S., Green, A. M., Trongsiriwat, N., Walsh, P. J., Klippenstein, S. J., and Lester, M.
419 I.: Four-Carbon Criegee Intermediate from Isoprene Ozonolysis: Methyl Vinyl Ketone Oxide Synthesis,
420 Infrared Spectrum, and OH Production, *J. Am. Chem. Soc.*, 140, 10866-10880,
421 <https://doi.org/10.1021/jacs.8b06010>, 2018.

422 Brown, S. S. and Stutz, J.: Nighttime Radical Observations and Chemistry, *Chem Soc Rev*, 41, 6405-
423 6447, <https://doi.org/10.1039/c2cs35181a>, 2012.

424 Capouet, M. and Müller, J. F.: A Group Contribution Method for Estimating the Vapour Pressures of α -
425 pinene Oxidation Products, *Atmos. Chem. Phys.*, 6, 1455-1467, <https://doi.org/10.5194/acp-6-1455-2006>, 2006.

427 Chen, Y., Tan, Y., Zheng, P., Wang, Z., Zou, Z., Ho, K. F., Lee, S., and Wang, T.: Effect of NO₂ on
428 Nocturnal Chemistry of Isoprene: Gaseous Oxygenated Products and Secondary Organic Aerosol
429 Formation, *Sci. Total Environ.*, 842, 156908, <https://doi.org/10.1016/j.scitotenv.2022.156908>, 2022.

430 Collaborators, G. B. D. R. F.: Global burden and strength of evidence for 88 risk factors in 204 countries
431 and 811 subnational locations, 1990-2021: a systematic analysis for the global burden of disease study
432 2021, *Lancet*, 403, 2162-2203, [https://doi.org/10.1016/S0140-6736\(24\)00933-4](https://doi.org/10.1016/S0140-6736(24)00933-4), 2024.

433 Compernolle, S., Ceulemans, K., and Müller, J. F.: EVAPORATION: a new vapour pressure estimation
434 method for organic molecules including non-additivity and intramolecular interactions, *Atmos. Chem.
435 Phys.*, 11, 9431-9450, <https://doi.org/10.5194/acp-11-9431-2011>, 2011.

436 Donahue, N. M., Tischuk, J. E., Marquis, B. J., and Huff Hartz, K. E.: Secondary organic aerosol from
437 limona ketone: insights into terpene ozonolysis via synthesis of key intermediates, *Phys Chem Chem
438 Phys*, 9, 2991-2998, <https://doi.org/10.1039/b701333g>, 2007.

439 Draper, D. C., Myllys, N., Hyttinen, N., Møller, K. H., Kjaergaard, H. G., Fry, J. L., Smith, J. N., and
440 Kurtén, T.: Formation of Highly Oxidized Molecules from NO₃ Radical Initiated Oxidation of Δ -3-
441 Carene: A Mechanistic Study, *ACS Earth Space Chem.*, 3, 1460-1470,
442 <https://doi.org/10.1021/acsearthspacechem.9b00143>, 2019.

443 Ehn, M., Thornton, J. A., Kleist, E., Sipila, M., Junninen, H., Pullinen, I., Springer, M., Rubach, F.,
444 Tillmann, R., Lee, B., Lopez-Hilfiker, F., Andres, S., Acir, I. H., Rissanen, M., Jokinen, T.,
445 Schobesberger, S., Kangasluoma, J., Kontkanen, J., Nieminen, T., Kurten, T., Nielsen, L. B., Jorgensen,
446 S., Kjaergaard, H. G., Canagaratna, M., Maso, M. D., Berndt, T., Petaja, T., Wahner, A., Kerminen, V.
447 M., Kulmala, M., Worsnop, D. R., Wildt, J., and Mentel, T. F.: A Large Source of Low-Volatility
448 Secondary Organic Aerosol, *Nature*, 506, 476-479, <https://doi.org/10.1038/nature13032>, 2014.

449 Fan, W., Chen, T., Zhu, Z., Zhang, H., Qiu, Y., and Yin, D.: A review of secondary organic aerosols

450 formation focusing on organosulfates and organic nitrates, *J. Hazard. Mater.*, 430, 128406,
451 <https://doi.org/10.1016/j.hazmat.2022.128406>, 2022.

452 Farmer, D. K., Matsunaga, A., Docherty, K. S., Surratt, J. D., Seinfeld, J. H., Ziemann, P. J., and Jimenez,
453 J. L.: Response of an Aerosol Mass Spectrometer to Organonitrates and Organosulfates and Implications
454 for Atmospheric Chemistry, *Proc. Natl. Acad. Sci. U.S.A.*, 107, 6670-6675,
455 <https://doi.org/10.1073/pnas.0912340107>, 2010.

456 Fisher, J. A., Jacob, D. J., Travis, K. R., Kim, P. S., Marais, E. A., Miller, C. C., Yu, K., Zhu, L., Yantosca,
457 R. M., Sulprizio, M. P., Mao, J., Wennberg, P. O., Crounse, J. D., Teng, A. P., Nguyen, T. B., St Clair, J.
458 M., Cohen, R. C., Romer, P., Nault, B. A., Wooldridge, P. J., Jimenez, J. L., Campuzano-Jost, P., Day, D.
459 A., Hu, W., Shepson, P. B., Xiong, F., Blake, D. R., Goldstein, A. H., Misztal, P. K., Hanisco, T. F., Wolfe,
460 G. M., Ryerson, T. B., Wisthaler, A., and Mikoviny, T.: Organic Nitrate Chemistry and Its Implications
461 for Nitrogen Budgets in An Isoprene- and Monoterpene-Rich Atmosphere: Constraints from Aircraft
462 (SEAC⁴RS) and Ground-Based (SOAS) Observations in the Southeast US, *Atmos. Chem. Phys.*, 16,
463 5969-5991, <https://doi.org/10.5194/acp-16-5969-2016>, 2016.

464 Fry, J. L., Draper, D. C., Barsanti, K. C., Smith, J. N., Ortega, J., Winkler, P. M., Lawler, M. J., Brown,
465 S. S., Edwards, P. M., Cohen, R. C., and Lee, L.: Secondary Organic Aerosol Formation and Organic
466 Nitrate Yield from NO₃ Oxidation of Biogenic Hydrocarbons, *Environ. Sci. Technol.*, 48, 11944-11953,
467 <https://doi.org/10.1021/es502204x>, 2014.

468 Fry, J. L., Kiendler-Scharr, A., Rollins, A. W., Brauers, T., Brown, S. S., Dorn, H. P., Dubé, W. P., Fuchs,
469 H., Mensah, A., Rohrer, F., Tillmann, R., Wahner, A., Wooldridge, P. J., and Cohen, R. C.: SOA from
470 Limonene: Role of NO₃ in Its Generation and Degradation, *Atmos. Chem. Phys.*, 11, 3879-3894,
471 <https://doi.org/10.5194/acp-11-3879-2011>, 2011.

472 Glasius, M. and Goldstein, A. H.: Recent Discoveries and Future Challenges in Atmospheric Organic
473 Chemistry, *Environ. Sci. Technol.*, 50, 2754-2764, <https://doi.org/10.1021/acs.est.5b05105>, 2016.

474 Guenther, A. B., Jiang, X., Heald, C. L., Sakulyanontvittaya, T., Duhl, T., Emmons, L. K., and Wang, X.:
475 The Model of Emissions of Gases and Aerosols from Nature version 2.1 (MEGAN2.1): an Extended and
476 Updated Framework for Modeling Biogenic Emissions, *Geosci. Model Dev.*, 5, 1471-1492,
477 <https://doi.org/10.5194/gmd-5-1471-2012>, 2012.

478 Guo, F., Bui, A. A. T., Schulze, B. C., Dai, Q., Yoon, S., Shrestha, S., Wallace, H. W., Sanchez, N. P.,
479 Alvarez, S., Erickson, M. H., Sheesley, R. J., Usenko, S., Flynn, J., and Griffin, R. J.: Airmass History,
480 Night-Time Particulate Organonitrates, and Meteorology Impact Urban SOA Formation Rate, *Atmos.*
481 *Environ.*, 322, <https://doi.org/10.1016/j.atmosenv.2024.120362>, 2024.

482 Guo, Y., Shen, H., Pullinen, I., Luo, H., Kang, S., Vereecken, L., Fuchs, H., Hallquist, M., Acir, I.-H.,
483 Tillmann, R., Rohrer, F., Wildt, J., Kiendler-Scharr, A., Wahner, A., Zhao, D., and Mentel, T. F.:
484 Identification of Highly Oxygenated Organic Molecules and Their Role in Aerosol Formation in the
485 Reaction of Limonene with Nitrate Radical, *Atmos. Chem. Phys.*, 22, 11323-11346,
486 <https://doi.org/10.5194/acp-22-11323-2022>, 2022.

487 Hallquist, M., Wängberg, I., Ljungström, E., Barnes, I., and Becker, K.-H.: Aerosol and Product Yields
488 from NO₃ Radical-Initiated Oxidation of Selected Monoterpenes, *Environ. Sci. Technol.*, 33, 553-559,
489 <https://doi.org/10.1021/es980292s>, 1999.

490 Ham, J. E., Harrison, J. C., Jackson, S. R., and Wells, J. R.: Limonene ozonolysis in the presence of nitric
491 oxide: Gas-phase reaction products and yields, *Atmos. Environ.* (1994), 132, 300-308,
492 <https://doi.org/10.1016/j.atmosenv.2016.03.003>, 2016.

493 Jokinen, T., Berndt, T., Makkonen, R., Kerminen, V. M., Junninen, H., Paasonen, P., Stratmann, F.,

494 Herrmann, H., Guenther, A. B., Worsnop, D. R., Kulmala, M., Ehn, M., and Sipila, M.: Production of
495 Extremely Low Volatile Organic Compounds from Biogenic Emissions: Measured Yields and
496 Atmospheric Implications, Proc. Natl. Acad. Sci. U.S.A., 112, 7123-7128,
497 <https://doi.org/10.1073/pnas.1423977112>, 2015.

498 Kiendler - Scharr, A., Mensah, A. A., Friese, E., Topping, D., Nemitz, E., Prevot, A. S. H., Äijälä, M.,
499 Allan, J., Canonaco, F., Canagaratna, M., Carbone, S., Crippa, M., Dall Osto, M., Day, D. A., De Carlo,
500 P., Di Marco, C. F., Elbern, H., Eriksson, A., Freney, E., Hao, L., Herrmann, H., Hildebrandt, L., Hillamo,
501 R., Jimenez, J. L., Laaksonen, A., McFiggans, G., Mohr, C., O'Dowd, C., Otjes, R., Ovadnevaite, J.,
502 Pandis, S. N., Poulain, L., Schlag, P., Sellegri, K., Swietlicki, E., Tiitta, P., Vermeulen, A., Wahner, A.,
503 Worsnop, D., and Wu, H. C.: Ubiquity of Organic Nitrates from Nighttime Chemistry in the European
504 Submicron Aerosol, Geophys. Res. Lett., 43, 7735-7744, <https://doi.org/10.1002/2016gl069239>, 2016.

505 Kilgour, D. B., Jernigan, C. M., Zhou, S., Brito de Azevedo, E., Wang, J., Zawadowicz, M. A., and
506 Bertram, T. H.: Contribution of Speciated Monoterpenes to Secondary Aerosol in the Eastern North
507 Atlantic, ACS Environ. Sci. Technol. Air, 555-566, <https://doi.org/10.1021/acsestair.3c00112>, 2024.

508 Kurten, T., Moller, K. H., Nguyen, T. B., Schwantes, R. H., Misztal, P. K., Su, L., Wennberg, P. O., Fry,
509 J. L., and Kjaergaard, H. G.: Alkoxy Radical Bond Scissions Explain the Anomalously Low Secondary
510 Organic Aerosol and Organonitrate Yields From alpha-Pinene + NO₃, J. Phys. Chem. Lett., 8, 2826-2834,
511 <https://doi.org/10.1021/acs.jpcllett.7b01038>, 2017.

512 Kwan, A. J., Chan, A. W. H., Ng, N. L., Kjaergaard, H. G., Seinfeld, J. H., and Wennberg, P. O.: Peroxy
513 Radical Chemistry and OH Radical Production during the NO₃-Initiated Oxidation of Isoprene, Atmos.
514 Chem. Phys., 12, 7499-7515, <https://doi.org/10.5194/acp-12-7499-2012>, 2012.

515 Lelieveld, J., Evans, J. S., Fnais, M., Giannadaki, D., and Pozzer, A.: The contribution of outdoor air
516 pollution sources to premature mortality on a global scale, Nature, 525, 367-371,
517 <https://doi.org/10.1038/nature15371>, 2015.

518 Li, Y., Fu, T. M., Yu, J. Z., Yu, X., Chen, Q., Miao, R., Zhou, Y., Zhang, A., Ye, J., Yang, X., Tao, S., Liu,
519 H., and Yao, W.: Dissecting the Contributions of Organic Nitrogen Aerosols to Global Atmospheric
520 Nitrogen Deposition and Implications for Ecosystems, Natl. Sci. Rev.,
521 <https://doi.org/10.1093/nsr/nwad244>, 2023a.

522 Li, Y., Fu, T. M., Yu, J. Z., Yu, X., Chen, Q., Miao, R., Zhou, Y., Zhang, A., Ye, J., Yang, X., Tao, S., Liu,
523 H., and Yao, W.: Dissecting the contributions of organic nitrogen aerosols to global atmospheric nitrogen
524 deposition and implications for ecosystems, Natl. Sci. Rev., 10, 244,
525 <https://doi.org/10.1093/nsr/nwad244>, 2023b.

526 Lin, G., Sillman, S., Penner, J. E., and Ito, A.: Global modeling of SOA: the use of different mechanisms
527 for aqueous-phase formation, Atmos. Chem. Phys., 14, 5451-5475, <https://doi.org/10.5194/acp-14-5451-2014>, 2014.

529 Liu, D., Zhang, Y., Zhong, S., Chen, S., Xie, Q., Zhang, D., Zhang, Q., Hu, W., Deng, J., Wu, L., Ma, C.,
530 Tong, H., and Fu, P.: Large Differences of Highly Oxygenated Organic Molecules (HOMs) and Low-
531 Volatile Species in Secondary Organic Aerosols (SOAs) Formed from Ozonolysis of β -pinene and
532 Limonene, Atmos. Chem. Phys., 23, 8383-8402, <https://doi.org/10.5194/acp-23-8383-2023>, 2023.

533 Luo, H., Vereecken, L., Shen, H., Kang, S., Pullinen, I., Hallquist, M., Fuchs, H., Wahner, A., Kiendler-
534 Scharr, A., Mentel, T. F., and Zhao, D.: Formation of Highly Oxygenated Organic Molecules from the
535 Oxidation of Limonene by OH Radical: Significant Contribution of H-abstraction Pathway, Atmos.
536 Chem. Phys., 23, 7297-7319, <https://doi.org/10.5194/acp-23-7297-2023>, 2023.

537 Matsunaga, A. and Ziemann, P. J.: Branching Ratios and Rate Constants for Decomposition and

538 Isomerization of beta-Hydroxyalkoxy Radicals Formed from OH Radical-Initiated Reactions of C₆-C₁₃
539 2-Methyl-1-Alkenes in the Presence of NO_x, J. Phys. Chem. A, 123, 7839-7846,
540 <https://doi.org/10.1021/acs.jpca.9b06218>, 2019.

541 Mayhew, A. W., Edwards, P. M., and Hamilton, J. F.: Daytime isoprene nitrates under changing NO_x and
542 O₃, Atmos. Chem. Phys., 23, 8473-8485, <https://doi.org/10.5194/acp-23-8473-2023>, 2023.

543 Mayorga, R., Xia, Y., Zhao, Z., Long, B., and Zhang, H.: Peroxy Radical Autoxidation and Sequential
544 Oxidation in Organic Nitrate Formation during Limonene Nighttime Oxidation, Environ. Sci. Technol.,
545 15337-15346, <https://doi.org/10.1021/acs.est.2c04030>, 2022.

546 McFiggans, G., Mentel, T. F., Wildt, J., Pullinen, I., Kang, S., Kleist, E., Schmitt, S., Springer, M.,
547 Tillmann, R., Wu, C., Zhao, D., Hallquist, M., Faxon, C., Le Breton, M., Hallquist, A. M., Simpson, D.,
548 Bergstrom, R., Jenkin, M. E., Ehn, M., Thornton, J. A., Alfarra, M. R., Bannan, T. J., Percival, C. J.,
549 Priestley, M., Topping, D., and Kiendler-Scharr, A.: Secondary organic aerosol reduced by mixture of
550 atmospheric vapours, Nature, 565, 587-593, <https://doi.org/10.1038/s41586-018-0871-y>, 2019.

551 Moldanova, J. and Ljungström, E.: Modelling of Particle Formation from NO₃ Oxidation of Selected
552 Monoterpenes, J. Aerosol Sci., 31, 1317-1333, [https://doi.org/10.1016/S0021-8502\(00\)00041-0](https://doi.org/10.1016/S0021-8502(00)00041-0), 2000.

553 Ng, N. L., Brown, S. S., Archibald, A. T., Atlas, E., Cohen, R. C., Crowley, J. N., Day, D. A., Donahue,
554 N. M., Fry, J. L., Fuchs, H., Griffin, R. J., Guzman, M. I., Herrmann, H., Hodzic, A., Iinuma, Y., Jimenez,
555 J. L., Kiendler-Scharr, A., Lee, B. H., Luecken, D. J., Mao, J., McLaren, R., Mutzel, A., Osthoff, H. D.,
556 Ouyang, B., Picquet-Varrault, B., Platt, U., Pye, H. O. T., Rudich, Y., Schwantes, R. H., Shiraiwa, M.,
557 Stutz, J., Thornton, J. A., Tilgner, A., Williams, B. J., and Zaveri, R. A.: Nitrate Radicals and Biogenic
558 Volatile Organic Compounds: Oxidation, Mechanisms, and Organic Aerosol, Atmos. Chem. Phys., 17,
559 2103-2162, <https://doi.org/10.5194/acp-17-2103-2017>, 2017.

560 Pankow, J. F. and Asher, W. E.: SIMPOL.1: a simple group contribution method for predicting vapor
561 pressures and enthalpies of vaporization of multifunctional organic compounds, Atmos. Chem. Phys., 8,
562 2773-2796, <https://doi.org/10.5194/acp-8-2773-2008>, 2008.

563 Perring, A. E., Pusede, S. E., and Cohen, R. C.: An Observational Perspective on the Atmospheric
564 Impacts of Alkyl and Multifunctional Nitrates on Ozone and Secondary Organic Aerosol, Chem. Rev.,
565 113, 5848-5870, <https://doi.org/10.1021/cr300520x>, 2013.

566 Picquet-Varrault, B., Suarez-Bertoa, R., Duncianu, M., Cazaunau, M., Pangui, E., David, M., and
567 Doussin, J.-F.: Photolysis and oxidation by OH radicals of two carbonyl nitrates: 4-nitrooxy-2-butanone
568 and 5-nitrooxy-2-pentanone, Atmos. Chem. Phys., 20, 487-498, <https://doi.org/10.5194/acp-20-487-2020>, 2020.

569 Pye, H. O., Luecken, D. J., Xu, L., Boyd, C. M., Ng, N. L., Baker, K. R., Ayres, B. R., Bash, J. O.,
570 Baumann, K., Carter, W. P., Edgerton, E., Fry, J. L., Hutzell, W. T., Schwede, D. B., and Shepson, P. B.:
571 Modeling the Current and Future Roles of Particulate Organic Nitrates in the Southeastern United States,
572 Environ. Sci. Technol., 49, 14195-14203, <https://doi.org/10.1021/acs.est.5b03738>, 2015.

573 Rollins, A. W., Kiendler-Scharr, A., Fry, J. L., Brauers, T., Brown, S. S., Dorn, H. P., Dubé, W. P., Fuchs,
574 H., Mensah, A., Mentel, T. F., Rohrer, F., Tillmann, R., Wegener, R., Wooldridge, P. J., and Cohen, R. C.:
575 Isoprene Oxidation by Nitrate Radical: Alkyl Nitrate and Secondary Organic Aerosol Yields, Atmos.
576 Chem. Phys., 9, 6685-6703, <https://doi.org/10.5194/acp-9-6685-2009>, 2009.

577 Sato, K., Inomata, S., Xing, J.-H., Imamura, T., Uchida, R., Fukuda, S., Nakagawa, K., Hirokawa, J.,
578 Okumura, M., and Tohno, S.: Effect of OH Radical Scavengers on Secondary Organic Aerosol Formation
579 from Reactions of Isoprene with Ozone, Atmos. Environ., 79, 147-154,
580 <https://doi.org/10.1016/j.atmosenv.2013.06.036>, 2013.

582 Shen, C., Yang, X., Thornton, J., Shilling, J., Bi, C., Isaacman-VanWertz, G., and Zhang, H.: Observation-
583 constrained kinetic modeling of isoprene SOA formation in the atmosphere, *Atmos. Chem. Phys.*, 24,
584 6153-6175, <https://doi.org/10.5194/acp-24-6153-2024>, 2024.

585 Shen, H., Zhao, D., Pullinen, I., Kang, S., Vereecken, L., Fuchs, H., Acir, I. H., Tillmann, R., Rohrer, F.,
586 Wildt, J., Kiendler-Scharr, A., Wahner, A., and Mentel, T. F.: Highly Oxygenated Organic Nitrates
587 Formed from NO₃ Radical-Initiated Oxidation of beta-Pinene, *Environ. Sci. Technol.*, 55, 15658-15671,
588 <https://doi.org/10.1021/acs.est.1c03978>, 2021.

589 Sindelarova, K., Granier, C., Bouarar, I., Guenther, A., Tilmes, S., Stavrakou, T., Müller, J. F., Kuhn, U.,
590 Stefani, P., and Knorr, W.: Global Data Set of Biogenic VOC Emissions Calculated by the MEGAN
591 Model over the last 30 years, *Atmos. Chem. Phys.*, 14, 9317-9341, <https://doi.org/10.5194/acp-14-9317-2014>, 2014.

592 Spittler, M., Barnes, I., Bejan, I., Brockmann, K. J., Benter, T., and Wirtz, K.: Reactions of NO₃ Radicals
593 with Limonene and α -pinene: Product and SOA Formation, *Atmos. Environ.*, 40, 116-127,
594 <https://doi.org/10.1016/j.atmosenv.2005.09.093>, 2006.

595 Surratt, J. D., Gómez-González, Y., Chan, A. W. H., Reinhilde, V., Mona, S., E, K. T., O, E. E., H, O. J.,
596 Michael, L., Mohammed, J., Willy, M., Magda, C., C, F. R., and H, S. J.: Organosulfate Formation in
597 Biogenic Secondary Organic Aerosol, *J. Phys. Chem. A*, 112, <https://doi.org/10.1021/jp802310p>, 2008.

598 Tao, J., Zhang, L., Cao, J., and Zhang, R.: A review of current knowledge concerning PM_{2.5} chemical
599 composition, aerosol optical properties and their relationships across China, *Atmos. Chem. Phys.*, 17,
600 9485-9518, <https://doi.org/10.5194/acp-17-9485-2017>, 2017.

601 Wang, Y., Takeuchi, M., Wang, S., Nizkorodov, S. A., France, S., Eris, G., and Ng, N. L.: Photolysis of
602 Gas-Phase Atmospherically Relevant Monoterpene-Derived Organic Nitrates, *J Phys Chem A*, 127, 987-
603 999, <https://doi.org/10.1021/acs.jpca.2c04307>, 2023.

604 Xu, L., Tsона, N. T., You, B., Zhang, Y., Wang, S., Yang, Z., Xue, L., and Du, L.: NO_x Enhances
605 Secondary Organic Aerosol Formation from Nighttime γ -terpinene Ozonolysis, *Atmos. Environ.*, 225,
606 <https://doi.org/10.1016/j.atmosenv.2020.117375>, 2020.

607 Yu, K., Zhu, Q., Du, K., and Huang, X.-F.: Characterization of Nighttime Formation of Particulate
608 Organic Nitrates Based on High-Resolution Aerosol Mass Spectrometry in an Urban Atmosphere in
609 China, *Atmos. Chem. Phys.*, 19, 5235-5249, <https://doi.org/10.5194/acp-19-5235-2019>, 2019.

610 Zang, H., Luo, Z., Li, C., Li, Z., Huang, D., and Zhao, Y.: Nocturnal Atmospheric Synergistic Oxidation
611 Reduces the Formation of Low-Volatility Organic Compounds from Biogenic Emissions, *Atmos. Chem.*
612 *Phys.*, 24, 11701-11716, <https://doi.org/10.5194/acp-24-11701-2024>, 2024.

613 Zare, A., Fahey, K. M., Sarwar, G., Cohen, R. C., and Pye, H. O. T.: Vapor-Pressure Pathways Initiate
614 but Hydrolysis Products Dominate the Aerosol Estimated from Organic Nitrates, *ACS Earth Space
615 Chem.*, 3, 1426-1437, <https://doi.org/10.1021/acsearthspacechem.9b00067>, 2019.

616 Zhao, D. F., Kaminski, M., Schlag, P., Fuchs, H., Acir, I. H., Bohn, B., Häseler, R., Kiendler-Scharr, A.,
617 Rohrer, F., Tillmann, R., Wang, M. J., Wegener, R., Wildt, J., Wahner, A., and Mentel, T. F.: Secondary
618 Organic Aerosol Formation from Hydroxyl Radical Oxidation and Ozonolysis of Monoterpenes, *Atmos.*
619 *Chem. Phys.*, 15, 991-1012, <https://doi.org/10.5194/acp-15-991-2015>, 2015.

620

621